JOURNAL OF COMPUTATIONAL PHYSICS 41, 270–294 (1981)

A Eulerian–Lagrangian Numerical Scheme for the Dispersion–Convection Equation Using Conjugate Space–Time Grids

SHLOMO P. NEUMAN

Department of Hydrology and Water Resources, University of Arizona, Tucson, Arizona 85721

Received July 28, 1980; revised October 23, 1980

A new numerical scheme is proposed for the dispersion–convection equation which combines the utility of a fixed grid in Eulerian coordinates with the computational power of the Lagrangian method. Convection is formally decoupled from dispersion in a manner which does not leave room for ambiguity. The resulting convection problem is solved by the method of characteristics on a grid fixed in space. Dispersion is handled by finite elements on a separate grid which may, but need not, coincide wit the former at selected points in space-time. Information is projected from one grid to another by local interpolation. The conjugate grid method is implemented by linear finite elements in conjunction with piecewise linear interpolation functions and applied to five problems ranging from predominant dispersion to pure convection. The results are entirely free of oscillations. Numerical dispersion exists but can be brought under control either by reducing the spatial increment, or by increasing the time step size, of the grid used to solve the convection problem. Contrary to many other methods, best results are often obtained when the Courant number exceeds 1.

1. INTRODUCTION

The dispersion–convection equation is widely used to describe Fickian transport of pollutants in the atmosphere, oceans, lakes, rivers, and subsurface bodies of water. In recent years, there has been much interest in the possibility of using this equation to predict the effect of groundwater flow on the migration of radionuclides from geological repositories of nuclear waste to the biosphere. This latter problem poses a special challenge to the numerical analyst because subsurface transport is often controlled by complex three-dimensional flow patterns which can vary with time, by an anisotropic dispersion process whose tensorial description depends on the velocity field, and by other complicating linear and nonlinear phenomena such as radioactive decay, sorption, and chemical reactions [1, 5, 6, 19, 20, 33].

The nature of the dispersion-convection equation can be conveniently characterized by the dimensionless Peclet number

$$Pe = |\mathbf{v}| L/D_m, \tag{1}$$

0021-9991/81/060270-25$02.00/0

where **v** is velocity vector, L is a characteristic length, and D_m is molecular diffusion. For example, in the case where an inert chemical species is spreading due to molecular diffusion in a one-dimensional velocity field, the governing equation can be written as

$$\frac{\partial c}{\partial t} = \frac{\partial^2 c}{\partial x^2} - Pe \frac{\partial c}{\partial x}, \tag{2}$$

where c is concentration, x is spatial coordinate defined relative to L, and t is time. Clearly, when Pe is small, dispersion dominates, and the equation is parabolic in character. When Pe is large, convection dominates, and the character of the equation changes to hyperbolic. In nonuniform flow fields where the velocity is not constant, Pe may vary from point to point both in space and time. As a result of this variation, the dispersion–convection equation may vary in character within a given field and with time, being predominantly parabolic in some regions and predominantly hyperbolic in others.

Most conventional numerical methods for solving the dispersion–convection equation can be classified into two major categories, Eulerian or Lagrangian, depending on the emphasis that they place on the parabolic or hyperbolic nature of the problem. In the Eulerian method, the governing equation is discretized by means of a finite difference or finite element grid fixed in space. Early experiments with finite differences [29, 36, 40] have shown that this technique performs well in dispersion-dominated situations at low Peclet numbers where the concentration function is relatively smooth. However, when the gradient of concentration is steep due to the prevalance of convection at high Pe, methods based on central difference approximations for the convection term may suffer from oscillations resulting in overshoot, undershoot, and negative concentrations. Price *et al.* [31] proved that such oscillations can be eliminated by restricting the size of the spatial grid increments; in the case of Eq. (2), the increments must satisfy $\Delta x \leqslant 2/Pe$. Since this is not always practical, the alternative is to use upstream difference approximations (also known as upstream weighting) which are able to eliminate oscillations, but they also introduce large truncation errors which are equivalent to a numerical (as opposed to physical) dispersion term [7, 21]. The effect of this numerical dispersion term is to smear sharp concentration fronts. Lantz [21] showed that for many practical problems, reducing numerical dispersion sufficiently so as to prevent masking phsyical dispersion may require an extremely fine grid. Another way to reduce numerical dispersion in upstream schemes is to cancel part of the truncation error by using higher-order approximations in space [9, 14, 23, 41], time [6–8, 45], or both [22]. Most of these have the effect of adding a negative correction term to the dispersion coefficient. A similar effect can also be achieved by means of flux corrections [4] or on the basis of physical considerations [43].

In recent years, there has been a growing belief that an alternative Eulerian approach for handling sharp fronts may be provided by high-order finite element techniques such as those proposed by Price *et al.* [32] and others [35, 44]. Price *et*

al. showed that high-order Galerkin approximations using smooth and nonsmooth Hermite polynomials are potentially far more accurate for a given amount of computational effort than standard finite difference techniques. Low-order finite element schemes also appear to be more accurate than standard finite differences [11, 39, 42]. However, in dealing with convection-dominated problems (especially the translation of square waves), the former are sometimes inferior when compared to the lowest-order flux-corrected finite difference scheme of Book *et al.* [4, 20]. Furthermore, time-centered finite element schemes suffer from oscillations, and backward difference schemes exhibit numerical dispersion [11, 42]. An upstream weighting finite element technique devised by Huyakorn [12, 15] reduces oscillations only at the expense of numerical smearing. So far, neither higher-order interpolations in space [42] nor in time [37] have proven capable of entirely eliminating both problems. Only a combination of high-order Hermite polynomials with a high-order approximation in time appears to provide a remedy to both ills [45].

Since standard Eulerian techniques are unsatisfactory, and the more complex techniques may not always be easily adapted to difficult problems, it is of interest to examine methods founded on the Lagrangian approach. Such methods are based either on a deforming grid or on a fixed grid in deforming coordinates. Varoğlu and Finn [47, 48] and Varoğlu [46] used space–time finite elements in one and two spatial dimensions, respectively, with sides paralleling either surfaces of constant time, or surfaces defined by characteristics. In this manner, the finite element equations become free of convective terms, resulting in a relatively wellbehaved diffusion-type problem. The idea is based on earlier uses of space–time finite elements in connection with the Stefan problem [2, 3] and equations representing conservation laws [16]. The method was tested by the authors on various problems ranging from dispersion-dominated cases to the pure convection of a rectangular wave. Their results did not show any oscillations and exhibited only a small amount of numerical dispersion in the case of pure convection. Another closely related approach is that described by O'Neill and Lynch [28] in which the nodal points of a one-dimensional Hermitian finite element grid are shifted during each time step parallel to the characteristics. The resulting finite element equations, which are coupled with finite differences in time, are thus devoid of convective terms and can be solved without difficulty. The authors demonstrated that when the grid is made fine enough in the vicinity of a sharp front, the results can be entirely free of oscillations or numerical dispersion. Not only are both methods highly accurate but, when convention dominates, both are also able to use large time steps such that the distance traveled by a fluid particle, say, Δs, is well in excess of the distance between contiguous nodal points, say, Δx. In many other methods, stability and convergence require that time step size be small enough to satisfy te Courant–Friedrichs–Lewy condition $\Delta s \leqslant \alpha \, \Delta x$ where α, the Courant number, is at most 1 [38]. Practical experience with various Eulerian schemes, including Hermitian finite elements, suggests that it is prudent to set α equal to $\frac{1}{3}$ [28].

Jensen [17] and Jensen and Finlayson [18] proposed a scheme in which the dispersion–convection equation is written in Lagrangian coordinates with origin at the

center of a moving front. When the velocity field is uniform, the equation becomes free of convective terms; otherwise, some residual first-order derivatives remain. By using orthogonal collocation on finite elements, the authors were able to obtain good results which showed no oscillations and only a minute amount of numerical dispersion at high Peclet numbers.

Even though these Lagrangian methods are more powerful than existing Eulerian techniques, they suffer from several limitations which may become serious when one considers complex problems such as the subsurface transport of nuclear waste. Since subsurface environments are often characterized by highly nonuniform material properties, the movement of nodal points across material interfaces may cause difficulties in the handling of equation parameters, especially if sorption and chemical reactions are important. Such movement may also result in severe grid deformations due to the refraction of streamlines across material interfaces, leading to numerical errors. When multiple sources exist, as in the case of chemical injection into the subsurface through several wells, concentration fronts may propagate in opposite directions and cross each other at various angles. This type of transport cannot be handled with the aid of deforming meshes or moving coordinates of the kind described above. Since velocities are usually computed independently of the transport problem by using a fixed Eulerian grid, it would be most convenient if the dispersion–convection equation could be solved on a grid compatible with the latter, especially when the velocity field varies with time. Finally, when the grid or the coordinates deform, the finite element matrices must be reevaluated and/or decomposed anew at every time step (in the case of Lagrangian coordinates, this is so because the boundary location varies with time); in linear problems solved on a Eulerian grid, the matrices remain constant, and if the time increment is fixed, a single LU-decomposition is enough.

The purpose of Eulerian–Lagrangian methods is to combine the simplicity of the fixed Eulerian grid with the computational power of the Lagrangian approach. Runca and Sardei [34] proposed to do this for horizontal advection and vertical eddy diffusion of air pollution by discretizing the vertical wind profile in a stepwise fashion. They then used different time intervals for each step so as to translate the concentration field to positions coincident with fixed Eulerian grid points during each time increment. Melli [24] solved the same problem with an irregular grid adapted to the wind profile so that the horizontal distance between nodes at each elevation is exactly equal to the distance traveled by a particle due to advection during a time step. Although his technique yielded good results for relatively large eddy diffusivities, attempts to propagate a sharp front met only with marginal success.

More interesting than the former is the particle tracking method originally suggested by Garder *et al.* [10] and later used extensively for subsurface transport [5, 19, 30, 33]. In this method, convection is handled by the method of characteristics applied to a set of moving particles. The dispersion part of the problem is solved by an explicit finite difference scheme on a fixed grid. In another version of the particle tracking method [1], dispersion is effected by means of a random walk process applied to each particle. Although both versions are virtually free of numerical

dispersion, they suffer from instability when the time step size exceeds a certain limit. The theory behind the particle tracking method is vague and therefore it cannot be shown to converge. The treatment of complex boundary conditions and nonlinearities is not straightforward, and implementation is complicated by the constant need to add particles at sources, eliminate them at sinks, and redistribute them in converging and diverging flow regimes.

In order to avoid the need for an independent set of moving particles, Hinstrup *et al.* [13] suggested redefining the particles at discrete time intervals so as to make them coincide with the nodes of a fixed finite difference grid. The position of each particle at intermediate times is obtained by polynomial interpolation between concentration values at neighboring grid points.

In the Eulerian–Lagrangian method proposed herein, convection is formally decoupled from dispersion in a manner which, contrary to previous such attempts [10, 13], does not leave room for ambiguity. Since the convection and dispersion problems require different treatments, they are solved on separate space–time grids. The nodes of these grids may, but need not, coincide at selected points. The spatial grids are fixed, but there is nothing in the method to prevent them from being deformable, if so desired. The method consists of solving the convection problem on one grid by the method of characteristics, projecting the result on the other grid by piecewise interpolation, solving the dispersion problem on this latter grid by finite elements, and finally projecting the result back on the first grid. A finite element approach based on the adaptive mixed explicit–implicit formulation [25–27] is shown to be particularly well suited for this problem.

The paper includes five one-dimensional examples covering the spectrum from dispersion-dominated problems to the pure convection of a rectangular wave. Even though projection from grid to grid in these examples is accomplished by piecewise linear interpolation, and the finite elements are constructed with piecewise linear basis functions, the results are entirely free of oscillations. Numerical dispersion exists but is kept under control by solving the convection problem on a grid having either sufficiently small spatial increments, or sufficiently large time increments. Not only is the time step size unaffected by the Courant–Friedrichs–Lewy condition but, in many cases, best results are obtained when the Courant number is well in excess of 1. Extension of the methodology to two- and three-dimensional problems requires further investigation.

2. THEORY

Consider the one-dimensional dispersion–convection equation

$$s(x,t)\frac{\partial c}{\partial t} = \frac{\partial}{\partial x}\left[D^*(x,t)\frac{\partial c}{\partial x} - v(x,t)c\right] - \lambda(x,t)c + q(x,t) \qquad \text{on} \quad (x_L, x_R)\times(0,\tau], \tag{3}$$

where c, x, and t are the same as in Eq. (2); D^* is dispersion coefficient; v is velocity; λ is decay coefficient; q is source term; s is retardation factor; x_L and x_R are left and right boundary points, respectively; and $(0, \tau]$ is time interval of interest. The parameters of Eq. (3) satisfy $D^* \geqslant 0$, $\lambda \geqslant 0$, and $s > 0$. The equation is to be solved for c, subject to the initial and boundary conditions

$$c(x, 0) = c_0(x) \qquad \text{on} \quad (x_L, x_R), \tag{4}$$

$$-D^* \frac{\partial c}{\partial x} + vc + \alpha_i(c - C_i) = Q_i \qquad \text{on} \quad x_i \in (0, \tau], \quad i = L, R \tag{5}$$

Here $c_0(x)$, $C_i(t)$, and $Q_i(t)$ are prescribed functions, and $\alpha_i(t)$ controls the type of boundary condition prevailing at $x_i \times (0, \tau]$: If $\alpha_i \to \infty$, Eq. (5) is a prescribed concentration condition; if $\alpha_i = 0$, it is a prescribed mass flux condition; otherwise, it is a mixed condition.

Since the retardation factor is assumed to satisfy $s(x, t) > 0$ for all $x, t \in (x_L, x_R) \times (0, \tau]$, one can define the hydrodynamic derivative, D/Dt, as

$$\frac{D}{Dt} = \frac{\partial}{\partial t} + \frac{v}{s}\frac{\partial}{\partial x}. \tag{6}$$

With the aid of this derivative, Eq. (3) can be rewritten in the form

$$s(x, t)\frac{Dc}{Dt} = \frac{\partial}{\partial x}\left[D^*(x, t)\frac{\partial c}{\partial x}\right] - f(x, t)c + q(x, t) \qquad \text{on} \quad (x_L, x_R) \times (0, \tau] \tag{7}$$

where $f = \partial v/\partial x + \lambda$. Here c no longer represents concentration at a point in space–time, but rather the concentration of a fictitious fluid particle moving at a velocity v/s. The pathline of this particle is described by the hydrodynamic derivative of x, which leads to the characteristic equation

$$Dx/v = Dt/s \qquad \text{on} \quad (x_L, x_R) \times (0, \tau]. \tag{8}$$

Equations (7)–(8) together with Eqs. (4)–(5) imply that $c(x, t)$ can be expressed as the sum of two functions, $\bar{c}(x, t)$ and $\mathring{c}(x, t)$, in the form

$$c = \bar{c} + \mathring{c}. \tag{9}$$

One way to define $\bar{c}$ is to require that it satisfy the homogeneous differential equation

$$D\bar{c}/Dt = 0 \qquad \text{on} \quad (x_L, x_R) \times (0, \tau] \tag{10}$$

subject to the initial condition

$$\bar{c}(x, 0) = c_0(x) \qquad \text{on} \quad (x_L, x_R) \tag{11}$$

and the Cauchy condition

$$v\bar{c} + \alpha_i(\bar{c} - C_i) = Q_i \qquad \text{on} \quad x_i \times (0, \tau]; \quad i = \text{L, R.} \tag{12}$$

Here x_i represents an inflow boundary at which fluid particles are entering the system; conditions at outflow boundaries have no effect on $\bar{c}$ and are therefore irrelevant. Clearly, the $\bar{c}$ value of a given fluid particle remains constant as the latter is convected through the flow field. The function $\dot{c}$ must then satisfy the equation

$$s(x,t)\frac{D\dot{c}}{Dt} = \frac{\partial}{\partial x}\left[D^*(x,t)\frac{\partial \dot{c}}{\partial x}\right] - f(x,t)\dot{c} + q(x,t) + \bar{g}(x,t) \qquad \text{on} \quad (x_\text{L}, x_\text{R}) \times (0, \tau], \tag{13}$$

where

$$\bar{g}(x,t) = \frac{\partial}{\partial x}\left[D^*(x,t)\frac{\partial \bar{c}}{\partial x}\right] - f(x,t)\bar{c}$$

subject to the initial and boundary conditions

$$\dot{c}(x,0) = 0 \qquad \text{on} \quad (x_\text{L}, x_\text{R}), \tag{14}$$

$$-D^*\frac{\partial \dot{c}}{\partial x} + (v + \alpha_i)\dot{c} = \bar{h} \qquad \text{on} \quad x_i \times (0, \tau], \quad i = \text{L, R}, \tag{15}$$

where $\bar{h}(x_i, t) = D^* \partial\bar{c}/\partial x$. If x_i is an outflow boundary at which particles are leaving the flow field, it is convenient to set $\alpha_i \to \infty$ so that Eq. (15) reduces to $\dot{c}(x_i, t) = 0$. This choice, though not necessary, is always possible due to the insensitivity of $\bar{c}$ to conditions prevailing at outflow boundaries. Note that Eqs. (13)–(15) are the same as Eqs. (7), (4), and (5), respectively. The fundamental difference is that in the former, $\bar{c}$ is treated as a known function, which is tantamount to saying that the effect of pure convection is known prior to solving Eqs. (13)–(15).

From the foregoing discussion we see that the original parabolic–hyperbolic dispersion–convection problem defined by Eqs. (3)–(5) can be formally decoupled into a purely hyperbolic problem defined by Eqs. (10)–(12), and another problem defined by Eqs. (13)–(15). The approach is to first solve the hyperbolic convection problem for $\bar{c}$, as the latter is independent of $\dot{c}$, and then solve the remaining problem for $\dot{c}$.

Another way to decompose c is to require that $\bar{c}$ satisfy the nonhomogeneous differential equation

$$s(x,t)\frac{D\bar{c}}{Dt} = -f(x,t)\bar{c} + q(x,t) \qquad \text{on} \quad (x_\text{L}, x_\text{R}) \times (0, \tau] \tag{16}$$

subject to Eqs. (11) and (12). When this is the case, $\dot{c}$ must satisfy

$$s(x,t)\frac{D\dot{c}}{Dt} = \frac{\partial}{\partial x}\left[D^*(x,t)\frac{\partial \dot{c}}{\partial x}\right] - f(x,t)\dot{c} + \bar{p}(x,t) \qquad \text{on} \quad (x_\text{L}, x_\text{R}) \times (0, \tau], \tag{17}$$

where

$$\bar{p}(x, t) = \frac{\partial}{\partial x}\left[D^*(x, t) \frac{\partial \bar{c}}{\partial x} \right]$$

subject to Eqs. (14) and (15). While this is a valid approach, it will not be pursued further in this text.

3. Eulerian–Lagrangian Numerical Method

3.1. *Conjugate Space–Time Grids*

In the numerical scheme proposed herein, the convection problem is solved for $\bar{c}$ by a stepwise method of characteristics, and the remaining problem is solved for $\hat{c}$ by finite elements. Since these two methods of solution are very different from each other, there is an advantage in using a different grid for each. The grid used for solving Eqs. (10)–(12) is referred to as "convection grid," and that used for Eqs. (13)–(15) is called "dispersion grid." Both grids are fixed in space and have distinct spatial and temporal increments. Their nodes may, but need not, coincide at selected points in space and time.

Figure 1 shows the particular conjugate space–time grids used in this paper. The spatial and temporal increments of the convection grid are Δx and Δt; those of the dispersion grid are $\Delta^\circ x$ and $\Delta^\circ t$. For reasons that will become obvious later, these increments are chosen such that $\Delta x \leqslant \Delta^\circ x$ and $\Delta t \geqslant \Delta^\circ t$. In addition, the grids are conveniently made to coincide at every $x_l = l\,\Delta^\circ x$ and $t_k = k\,\Delta t$, where l, $k = 0, 1, 2, \ldots$. Although the discretization intervals in Fig. 1 are constant, there is nothing in the theory or the method to prevent them from being variable in both space and time.

Let $\mathbf{c}^k$ be the vector of nodal c values on the convection grid at time t_k. Assume that $\mathbf{c}^k$ is known; we desire to compute $\mathbf{c}^{k+1}$ corresponding to a later time, $t_{k+1} = t_k + \Delta t$. We will accomplish this in two stages: first by evaluating $\bar{c}$ on the

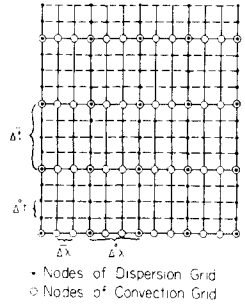

FIG. 1. Overlapping convection and dispersion grids.

convection grid at t_{k+1} by the method of characteristics and projecting it onto the dispersion grid, and then by evaluating $\mathring{c}$ on the dispersion grid at t_{k+1} by finite elements and projecting it back onto the convection grid so as to obtain $\bar{c} + \mathring{c}$.

3.2. *Convection by Method of Characteristics*

In most non-Eulerian techniques mentioned earlier, the method of characteristics is implemented by tracking the movement of fluid particles across the entire flow field, from the time they enter at a source, until they leave at a sink. In some of these techniques [17, 18, 28, 46–48] the particles coincide with nodal points, thereby causing either the grid or the coordinates to deform permanently with time.

In the method described below, the particles are redefined at every time step, $\overline{\Delta t}$, so as to coincide with the nodes of our fixed convection grid. At the beginning of a time step starting at t_k, the nodes of the convection grid are designated as moving particles. The pathline of each such nodal particle during the time interval $(t_k, t_{k+1}]$ can be charted out through integration of Eq. (8). If the position of the nth nodal particle at time t_k is x_n then, according to Eq. (8), its position at time t_{k+1} will be

$$x_n^{k+1} = x_n + \int_{t_k}^{t_{k+1}} \frac{v}{s}\, Dt. \tag{18}$$

Since v and s are given, x_n^{k+1} can be determined explicitly for every node n.

In the particular case where v/s = constant, or when $\overline{\Delta t}$ is small, the characteristics are straight lines or can be approximated as such. This situation is illustrated in Fig. 2. The figure shows that during the time step $\overline{\Delta t}$ each nodal particle, n, is translated from its old position, x_n, to a new position, x_n^{k+1}, along a straight line segment representing the characteristic passing through the point x_n at time t_k. This causes a temporary deformation of the convection grid (temporary because the results will be eventually projected back onto the original fixed grid points in the manner described below). Let $\bar{c}(x_n^{k+1}, t_{k+1})$ be the value of $\bar{c}$ at the new location, x_n^{k+1}, of a particle originating at x_n. Then by virtue of Eqs. (10) and (11),

$$\bar{c}(x_n^{k+1}, t_{k+1}) = c_n^k, \tag{19}$$

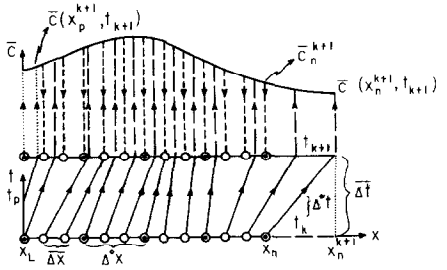

FIG. 2. Method of characteristics illustrated for constant v.

where c_n^k is c at (x_n, t_k). According to Eq. (12), the value of $\bar{c}$ at the inflow boundary, x_L in Fig. 2, is given by

$$\bar{c}(x_L, t_{k+1}) = \left. \frac{Q_L + \alpha_L C_L}{v + \alpha_L} \right|_{t=t_{k+1}} \tag{20}$$

On the basis of these point values, the function $\bar{c}(x, t_{k+1})$ can be approximated by a suitable interpolation formula over the entire flow domain $[x_L, x_R]$. If $n = 1$ is the node corresponding to x_L, and if $|x_1^{k+1} - x_L| > \Delta^\circ x$, it may sometimes be required to obtain additional values of $\bar{c}(x, t_{k+1})$ at one or more points $x_p^{k+1} \in (x_L, x_1^{k+1})$ for the interpolation to be sufficiently accurate. This can be done by allowing individual particles, p, to enter the system across x_L at one or more values of time, $t_p \in (t_k, t_{k+1})$, such that

$$x_p^{k+1} = x_L + \int_{t_p}^{t_{k+1}} \frac{v}{s} Dt \tag{21}$$

as shown in Fig. 2. This measure is needed only if the boundary condition at x_L varies with time during Δt.

After $\bar{c}(x, t_{k+1})$ is approximated by an appropriate interpolation formula, the function is projected onto the locations of the nodes representing the fixed convection and dispersion grids. This is equivalent to removing the effect of grid deformation. The procedure is illustrated in Fig. 2. The result is a set of nodal values, $\bar{c}_n^{k+1}$, of $\bar{c}$ at every x_n at time t_{k+1}. The particular computational results described below were obtained by piecewise linear interpolation. Additional possibilities worth exploring in the future include the use of cubic splines or other higher-order interpolation schemes.

If v/s varies with x and/or t, one may either treat it as a constant for the duration of Δt, or evaluate the integrals in Eq. (18) and (21) numerically by a suitable method such as Gaussian quadrature. In the latter case, the characteristics will no longer be straight lines but curves of arbitrary shape. This does not pose much difficulty because the form of the characteristics has no effect on our numerical procedure; only the final position of each nodal particle, x_n^{k+1}, is important. We may conclude that the magnitude of Δt is not restricted by the configuration of the pathlines. As a matter of contrast, Varoğlu and Finn [47, 48] use space–time finite elements having sides formed by characteristic curves. In complex flow fields, their approach may require keeping the time step small enough so as to enable approximating the element sides by polynomials of a sufficiently low degree.

3.3. *Dispersion by Finite Elements*

For the purpose of solving Eqs. (13)–(15), it is convenient to identify each point, $x \in [x_L, x_R]$, in the flow domain with a particle having reached the point x at time t_{k+1}. In particular, let x_n be the location of the nth node in the convection grid, and let N be the total number of such nodes. Similarly, let x_p be the location of the pth

node in the dispersion grid, and let P be the total number of these nodes. Then each node, n and p, is identified with a particle having reached the point x_n or x_p at time t_{k+1}.

Equations (13)–(15) can be solved for $\dot{c}$ by a finite element method applied over the dispersion grid. Other possible methods of solution not explored in this paper include explicit or implicit finite differences, integrated finite differences, and point collocation. We shall approximate the function $\bar{c}(x, t)$ by $\bar{c}^N(x, t)$ according to

$$\bar{c}(x, t) \approx \bar{c}^N(x, t) = \sum_{n=1}^{N} \bar{c}_n(t)\, \bar{\xi}_n(x), \tag{22}$$

where $\bar{c}_n$ are nodal values of $\bar{c}$ along the convection grid, and $\bar{\xi}_n$ are prescribed basis functions satisfying $\bar{\xi}_n(x_m) = \delta_{nm}$, the latter being the Kronecker delta (i.e., $\delta_{nm} = 1$ if $n = m$ and $\delta_{nm} = 0$ if $n \neq m$). Similarly, we shall approximate $\dot{c}(x, t)$ by $\dot{c}^P(x, t)$ according to

$$\dot{c}(x, t) \approx \dot{c}^P(x, t) = \sum_{p=1}^{P} \dot{c}_p(t)\, \dot{\xi}_p(x), \tag{23}$$

where $\dot{c}_p$ are nodal values of $\dot{c}$ along the dispersion grid, and $\dot{\xi}_p$ are prescribed basis functions satisfying $\dot{\xi}_p(x_r) = \delta_{pr}$. Application of the Galerkin orthogonalization process to Eq. (13) gives

$$\int_{x_L}^{x_R} \left\{ s \frac{D\dot{c}}{Dt} - \frac{\partial}{\partial x}\left[D^* \frac{\partial(\bar{c}^N + \dot{c}^P)}{\partial x} \right] + f(\bar{c}^N + \dot{c}^P) - q \right\} \dot{\xi}_p \, dx = 0, \qquad p = 1, 2, 3, \ldots, P, \tag{24}$$

where the time derivative is treated for the moment as a known function. Integration by parts yields

$$\int_{x_L}^{x_R} \left\{ \left[s \frac{D\dot{c}}{Dt} + f(\bar{c}^N + \dot{c}^P) - q \right] \dot{\xi}_p + D^* \frac{\partial(\bar{c}^N + \dot{c}^P)}{\partial x} \frac{\partial \dot{\xi}_p}{\partial x} \right\} dx + \delta_{Lp} D^* \frac{\partial(\bar{c}^N + \dot{c}^P)}{\partial x}\bigg|_{x=x_L} - \delta_{Rp} D^* \frac{\partial(\bar{c}^N + \dot{c}^P)}{\partial x}\bigg|_{x=x_R} = 0, \qquad p = 1, 2, \ldots, P, \tag{25}$$

where L and R are the nodes at x_L and x_R, respectively.

As will be seen below. by regarding each node as a moving particle, the resulting problem for $\dot{c}$ will become purely parabolic in nature. It has been shown [26] that for such parabolic problems, there is an advantage in adopting the so-called lumped-mass finite element approach, in which the first integral on the left side of Eq. (25) is approximated by

$$\int_{x_L}^{x_R} s \frac{D\dot{c}}{Dt} \dot{\xi}_p \, dx \approx \frac{D\dot{c}_p}{Dt} \int_{x_L}^{x_R} s \dot{\xi}_p \, dx. \tag{26}$$

Note that this is analogous to what one does in most conventional finite difference schemes. Substituting Eqs. (15), (22), (23), and (26) into (25) leads to the following system of ordinary differential equations,

$$(\mathbf{A} + \mathbf{B} + \mathbf{F})\dot{\mathbf{c}} + \mathbf{S}\frac{D\dot{\mathbf{c}}}{Dt} = \mathbf{Q}. \tag{27}$$

Here $\mathbf{A}$ is a symmetric positive-definite "dispersion matrix" of order P whose p, rth term is defined as

$$A_{pr} = \int_{x_L}^{x_R} D^* \frac{\partial \mathring{\xi}_p}{\partial x}\frac{\partial \mathring{\xi}_r}{\partial x}\,dx. \tag{28}$$

$\mathbf{B}$ is a diagonal "boundary matrix" of order P, whose terms are

$$\begin{aligned} B_{pr} &= (\delta_{Lp} - \delta_{Rp})(v|_{x=x_p} + \alpha_p), \qquad && \alpha_p < \infty, \\ B_{pp} &= 0, && \alpha_p \to \infty. \end{aligned} \tag{29}$$

$\mathbf{F}$ is a square symmetric matrix of order P defined by

$$F_{pr} = \int_{x_L}^{x_R} f\mathring{\xi}_p\mathring{\xi}_r\,dx. \tag{30}$$

$\dot{\mathbf{c}}$ is the P-dimensional vector of $\dot{c}_p$ values. $\mathbf{S}$ is a diagonal "retardation matrix" of order P having the terms

$$S_{pp} = \int_{x_L}^{x_R} c\mathring{\xi}_p\,dx \tag{31}$$

Finally, $\mathbf{Q}$ is a "source vector" defined as

$$Q_p = \beta_p + \int_{x_L}^{x_R} q\mathring{\xi}_p\,dx - \sum_{n=1}^{N} \bar{c}_n \int_{x_L}^{x_R} \left(f\bar{\xi}_n\mathring{\xi}_p + D^*\frac{\partial \bar{\xi}_n}{\partial x}\frac{\partial \mathring{\xi}_p}{\partial x}\right) dx, \tag{32}$$

where

$$\begin{aligned} \beta_p &= 0, && \alpha_p < \infty, \\ \beta_p &= (\delta_{Rp} - \delta_{Lp})\,D^*\frac{\partial(\bar{c} + \dot{c})}{\partial x}\bigg|_{x=x_p}, && \alpha_p \to \infty. \end{aligned} \tag{33}$$

Note that when $\alpha_p \to \infty$, $\dot{c}_p$ is known to be zero by virtue of Eq. (15), and the pth row of Eq. (27) is not needed to compute $\dot{\mathbf{c}}$. Thus, β_p need not be evaluated from Eq. (33), but can be obtained a posteriori from Eq. (27) after $\dot{\mathbf{c}}$ has been computed, if so desired.

The computational results described later in the text were obtained with the aid of piecewise linear "chapeau" basis functions [32] defined as

$$\begin{aligned} \bar{\xi}_n(x) &= \bar{\xi}_{n-}(x) \cup \bar{\xi}_{n+}(x), \\ \mathring{\xi}_p(x) &= \mathring{\xi}_{p-}(x) \cup \mathring{\xi}_{p+}(x), \end{aligned} \tag{34}$$

where

$$\bar{\xi}_{n-}(x) = \frac{x - x_{n-1}}{x_n - x_{n-1}}, \qquad x \in [x_{n-1}, x_n],$$

$$\bar{\xi}_{n+}(x) = \frac{x_{n+1} - x}{x_{n+1} - x_n}, \qquad x \in [x_n, x_{n+1}],$$

$$\mathring{\xi}_{p-}(x) = \frac{x - x_{p-1}}{x_p - x_{p-1}}, \qquad x \in [x_{p-1}, x_p],$$

$$\mathring{\xi}_{p+}(x) = \frac{x_{p+1} - x}{x_{p+1} - x_p}, \qquad x \in [x_p, x_{p+1}],$$

and $x_L = x_1 < x_2 < \cdots < x_n < \cdots < x_{N-1} < x_N = x_R$ as well as $x_L = x_1 < x_2 < \cdots < x_p < \cdots < x_{P-1} < x_P = x_R$. By assuming that D^*, f, s, and q are uniform within any given element of the dispersion grid, the integrals in Eqs. (28) and (30)–(32) are easily evaluated:

$$\begin{aligned} A_{pr} &= -\frac{D^*_{\mathring{e}}}{L_{\mathring{e}}}\gamma_{pr}, \qquad p \neq r, \\ A_{pp} &= -\sum_{r \neq p} A_{pr}, \\ \gamma_{pr} &= 1 \qquad \text{if } p \text{ and } r \text{ are contiguous nodes} \\ &= 0 \qquad \text{otherwise,} \end{aligned} \tag{35}$$

where $\mathring{e}$ is the element of the dispersion grid defined by x_p and x_r, $D^*_{\mathring{e}}$ is the value of D^* in $\mathring{e}$, and $L_{\mathring{e}}$ is the length of $\mathring{e}$ (equal to $\Delta^\circ x$ in Figs. 1 and 2);

$$\begin{aligned} F_{pr} &= \tfrac{1}{6} f_{\mathring{e}} L_{\mathring{e}} \gamma_{pr}, \qquad p \neq r, \\ F_{pp} &= 2 \sum_{r \neq p} F_{pr}, \end{aligned} \tag{36}$$

where $f_{\mathring{e}}$ is the value of f in $\mathring{e}$;

$$S_{pp} = \tfrac{1}{2} \sum_{\mathring{e}} s_{\mathring{e}} L_{\mathring{e}}, \tag{37}$$

where $s_{\dot{e}}$ is the value of s in $\dot{e}$ and the summation is taken over the two elements contiguous with p; and

$$Q_p = \beta_p + \tfrac{1}{2} \sum_{\dot{e}} q_{\dot{e}} L_{\dot{e}} - \sum_{n=1}^{N} G_{pn} \bar{c}_n, \tag{38}$$

where $q_{\dot{e}}$ is the value of q in $\dot{e}$ and, for the case where each $\Delta^\circ x$ contains an integer number of $\overline{\Delta x}$'s as in Fig. 1,

$$\begin{aligned}
G_{pn} &= \sum_{\dot{e}} \left[\frac{f_{\dot{e}} L_{\bar{e}}^2}{6 L_{\dot{e}}} \left(3 \frac{L_{\dot{e}}}{L_{\bar{e}}} - 1 \right) + \frac{D^*_{\dot{e}}}{L_{\dot{e}}} \right] && \text{if} \quad x_n = x_p \\
&= f_{\dot{e}} \frac{L_{\bar{e}}}{L_{\dot{e}}} (x_n - x_{p-1}) && \text{if} \quad x_{p-1} < x_n < x_p \\
&= f_{\dot{e}} \frac{L_{\bar{e}}}{L_{\dot{e}}} (x_{p+1} - x_n) && \text{if} \quad x_p < x_n < x_{p+1} \\
&= \frac{f_{\dot{e}} L_{\bar{e}}^2}{6 L_{\dot{e}}} - \frac{D^*_{\dot{e}}}{L_{\dot{e}}} && \text{if} \quad x_n = x_{p-1}, x_{p+1}.
\end{aligned}$$

Here $L_{\bar{e}}$ is the length of each element of the convection grid lying inside $\dot{e}$ (equal to $\overline{\Delta x}$ in Figs. 1 and 2), and the summation is taken over the two elements contiguous with p. Better accuracy could probably be achieved with higher-order basis functions and a more precise description of the manner in which D^*, f, s, and q vary in space.

The differential matrix equation (27) will be integrated in time by finite differences. If this integration would take place at nodal points fixed in space, the hydrodynamic derivative $D\dot{\mathbf{c}}/Dt$ would have to be expressed as the sum of a partial derivative $\partial\dot{\mathbf{c}}/\partial t$ and a convective term. In order to avoid dealing with such a convective term, we will perform the time integration in a manner which is analogous to solving Eq. (27) along the characteristics defined by Eq. (8). The resulting problem will thus have a purely parabolic nature, and will involve only symmetric and diagonal matrices.

Let $\dot{\mathbf{c}}^{k,j}$ be the value of $\dot{\mathbf{c}}$ at time $t_{k,j} = t_k + j\Delta^\circ t$, where $j = 1, 2, \ldots, J$ and $J\Delta^\circ t = \overline{\Delta t}$ so that $\dot{\mathbf{c}}^{k,J} = \dot{\mathbf{c}}^{k+1}$. As mentioned earlier, we assume that all nodes n of the fixed convection grid, and all nodes p of the fixed dispersion grid, are moving particles having reached their respective positions at time t_{k+1}. If n and p were not particles but fixed points in space, $\bar{c}_n$ and $\bar{c}_p$ would generally vary during $\overline{\Delta t}$. If, however, we set $\bar{c}_n$ and $\bar{c}_p$ equal to $\bar{c}_n^{k+1}$ and $\bar{c}_p^{k+1}$ for the duration of $\overline{\Delta t}$ then we are implying, by virtue of Eq. (10), that n and p are particles that have traveled along their respective characteristics and reached their current positions at time t_{k+1}. Since the only term involving $\bar{c}$ in Eq. (27) is $\mathbf{Q}$, it is enough to evaluate $\mathbf{Q}$ in Eqs. (32) and (38) in terms of $\bar{c}^{k+1}$. We will designate the resulting value of $\mathbf{Q}$ by $\mathbf{Q}^{k+1}$.

In order to avoid tracing the actual path taken by each nodal particle during $\overline{\Delta t}$, it is convenient to evaluate the matrices $\mathbf{A}$, $\mathbf{B}$, $\mathbf{F}$, and $\mathbf{S}$ in Eq. (27) only at the end of

the time step when the particle locations are known. This leads to the following finite difference equivalent of Eq. (27),

$$(\mathbf{A}+\mathbf{B}+\mathbf{F})^{k+1}\,[\theta\mathring{\mathbf{c}}^{k,j}+(1-\theta)\,\mathring{\mathbf{c}}^{k,j-1}] + \mathbf{S}^{k+1}(\mathring{\mathbf{c}}^{k,j}-\mathring{\mathbf{c}}^{k,j-1})/\Delta^{\circ}t=\mathbf{Q}^{k+1}, \qquad 0<j\leqslant J, \tag{39}$$

where $0\leqslant\theta\leqslant 1$. Since at t_k the function $\bar{c}$ is set equal to c, Eq. (14) implies that $\mathring{\mathbf{c}}^{k,0}=0$. This provides the initial condition needed for solving Eq. (39) for $\mathring{\mathbf{c}}^{k,j}$ from $j=1$ to J. Note that in the particular case where $J=1$ and $\theta=1$, Eq. (39) reduces to a simple backward difference scheme valid along characteristics passing through the fixed nodal points of the two conjugate grids. After solving Eq. (39) for $\mathring{c}_p^{k+1}$ at all nodes, p, of the dispersion grid, one can use Eq. (23) to compute $\mathring{c}_n^{k+1}$ at each node, n, of the convection grid according to

$$\mathring{c}_n^{k+1}=\sum_{p=1}^{P}\mathring{c}_p^{k+1}\mathring{\xi}_p(x_n). \tag{40}$$

The final concentration at the nodes of both grids is then given by

$$\begin{aligned}\mathring{c}_p^{k+1}&=\bar{c}_p^{k+1}+\mathring{c}_p^{k+1}, \qquad p=1,2,\ldots,P,\\ \mathring{c}_n^{k+1}&=\bar{c}_n^{k+1}+\mathring{c}_n^{k+1}, \qquad n=1,2,\ldots,N.\end{aligned} \tag{41}$$

A few additional remarks concerning Eq. (39) are in order. Consider the pth row of this equation,

$$\sum_{r=1}^{P}(A_{pr}+B_{pr}+F_{pr})^{k+1}\,[\theta\mathring{c}_r^{k,j}+(1-\theta)\,\mathring{c}_r^{k,j-1}] + S_{pp}^{k+1}(\mathring{c}_p^{k,j}-\mathring{c}_p^{k,j-1})/\Delta^{\circ}t=Q_p^{k+1}, \qquad 0<j\leqslant J. \tag{42}$$

When $\theta=0$, Eq. (42) can be solved explicitly for $\mathring{c}_p^{k,j}$ (this is a direct consequence of the lumped-mass approximation in Eq. (26)). Neuman and Narasimhan [26] proved that such a solution will be stable provided only that

$$\frac{\Delta^{\circ}t}{S_{pp}}(A_{pp}+B_{pp}+F_{pp})\leqslant 1 \tag{43}$$

and

$$A_{pp}+B_{pp}+F_{pp}\geqslant\sum_{r\neq p}|A_{pr}+B_{pr}+F_{pr}|. \tag{44}$$

Thus, the problem can be solved explicitly at nodes satisfying the above criteria for a given $\Delta^{\circ}t$, and implicitly at all other nodes. This leads to an adaptive mixed explicit–implicit approach which results in improved computation efficiency when dealing with nonuniform flow fields and parameters varying in space [25–27].

Experience shows that in order to prevent oscillations, the c values at nodes of the convection grid lying in the interior of a given element of the dispersion grid must vary monotonically between the values at the element end points. When this is not the case, as may happen on a few occasions, the interior c values must be modified so as to satisfy this requirement. In this paper, the interior c values were made to vary linearly between the nodes of the dispersion grid whenever one of them exceeded the largest, or fell below the smallest, c values at the edges of an element. There is little doubt that this arbitrary smoothing may cause some numerical dispersion, although the primary cause of such dispersion is the interpolation of c values as described earlier in connection with Fig. 2. Fortunately, we will be able to demonstrate later that numerical dispersion is amenable to control either by reducing $\overline{\Delta x}$ or by increasing $\overline{\Delta t}$.

As stated earlier, Eqs. (13)–(15) are the same as Eqs. (7), (4), and (5), respectively. Thus, instead of solving the former for $\mathring{c}$ one could, in principle, solve the latter for c. However, posing the problem in terms of $\mathring{c}$ has an advantage: In many cases, $\mathring{c}$ varies much more slowly in space than c and, therefore, can be approximated by means of low-order basis functions defined on a relatively coarse finite element grid.

4. Reversing the Solution Sequence

The methodology described in Section 3 of this paper requires that, during each $\overline{\Delta t}$, $\bar{c}$ be calculated by the method of characteristics prior to computing $\mathring{c}$ by finite elements. This means that the concentration profile is first translated parallel to the characteristics, and only then allowed to disperse. Another possibility is to reverse the sequence of the solutions by allowing the profile to disperse before it is translated in the direction of the flow. For this purpose, it is convenient to treat all nodes, n, of the fixed convection grid, and all nodes, p, of the fixed dispersion grid, as particles about to move away from their respective positions at time t_k. According to Eqs. (10) and (11), $\bar{c}_n$ and $\bar{c}_p$ must remain equal to c_n^k and c_p^k, respectively, during the entire time interval $\overline{\Delta t}$. This requirement can be satisfied by evaluating $\mathbf{Q}$ in Eqs. (32) and (38) in terms of c_n^k. We will designate the resulting value of $\mathbf{Q}$ by $\mathbf{Q}^k$.

In order to avoid tracing the actual path that each nodal particle will take during $\overline{\Delta t}$, the matrices $\mathbf{A}$, $\mathbf{B}$, $\mathbf{F}$, and $\mathbf{S}$ are evaluated at the beginning of the time step when the particle locations are knwon. This leads to the following finite difference expression for Eq. (27):

$$(\mathbf{A}+\mathbf{B}+\mathbf{F})^k\,[\theta\mathring{\mathbf{c}}^{k,j}+(1-\theta)\,\mathring{\mathbf{c}}^{k,j-1}] + \mathbf{S}^k(\mathring{\mathbf{c}}^{k,j}-\mathring{\mathbf{c}}^{k,j-1})/\Delta^{\circ}t=\mathbf{Q}^k, \qquad 0<j\leqslant J. \tag{45}$$

Since at t_k the function $\bar{c}$ is set equal to c, Eq. (14) implies that $\mathring{\mathbf{c}}^{k,0}=0$, which provides the necessary initial condition for Eq. (45). Note that in the particular case where $J=1$ and $\theta=0$, the latter equation reduces to an explicit forward difference

scheme valid along characteristics passing through the fixed nodes of the two conjugate grids.

After solving Eq. (45) for $\mathring{c}_p^{k+1}$ at all nodes, p, of the dispersion grid, one can use Eq. (40) to compute $\mathring{c}_n^{k+1}$ at each node, n, of the convection grid. The total concentrations at p and n, prior to translation, are therefore $(c_p^k + \mathring{c}_p^{k+1})$ and $(c_n^k + \mathring{c}_n^{k+1})$, respectively. These values must now be translated along the characteristics, and then projected back onto the fixed locations of both sets of nodes, in the same manner as that explained earlier in connection with $\bar{c}$ (see Fig. 2).

The question of which is preferable, translation first and dispersion second, or dispersion first and translation second, will receive a preliminary answer in the following section.

5. Examples

The following five examples show how the conjugate grid method performs under a variety of conditions. All the results were obtained by using piecewise linear interpolation and time-centered ($\theta = 0.5$) linear finite elements with chapeau basis functions. The results quoted for Examples 1–4 were obtained by using the method of translation first, dispersion second, during each Δt. The results quoted for Example 5 were obtained by reversing this sequence of operations.

Example 1 concerns the problem of solving

$$\frac{\partial c}{\partial t} = D^* \frac{\partial^2 c}{\partial x^2} - v \frac{\partial c}{\partial x} \qquad \text{on} \quad (0, x_R) \times (0, \tau] \tag{46}$$

subject to

$$c(x, 0) = 0 \qquad \text{on} \quad (0, x_R), \tag{47}$$

$$\begin{aligned} c(0, t) &= 1 \qquad \text{on} \quad (0, \tau], \\ c(x_R, t) &= 0 \qquad \text{on} \quad (0, \tau]. \end{aligned} \tag{48}$$

[illegible]

strongly dispersion-dominated with a Peclet number $Pe = vx_R/D^* = 12.5$. The results for $t = 2$, 6, and 10 are shown in Fig. 3. They are seen to compare very well with the analytical solution,

$$c(x, t) = \frac{1}{2} \operatorname{erfc}\left(\frac{x - vt}{2\sqrt{D^* t}}\right) + \frac{1}{2} \exp\left(\frac{vx}{D^*}\right) \operatorname{erfc}\left(\frac{x + vt}{2\sqrt{D^* t}}\right), \tag{49}$$

which is valid for $x_R \to \infty$. Similar results were obtained for this problem by Varoğlu and Finn [47].

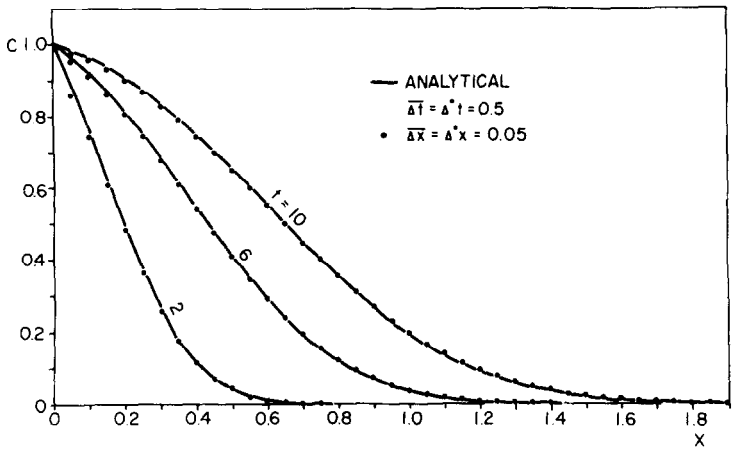

FIG. 3. Results of Example 1.

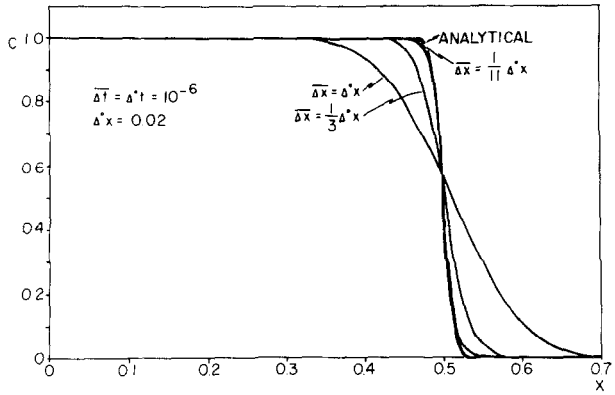

FIG. 4. Results of Example 2 for $t = 5 \times 10^{-5}$ using $\overline{\Delta t} = \Delta^\circ t = 10^{-6}$.

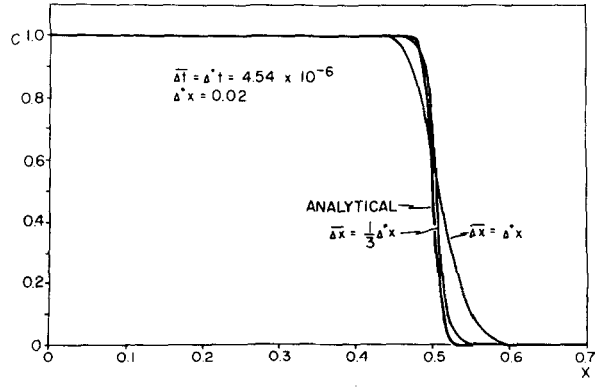

FIG. 5. Results of Example 2 for $t = 5 \times 10^{-5}$ using $\overline{\Delta t} = \Delta^\circ t = 4.54 \times 10^{-6}$.

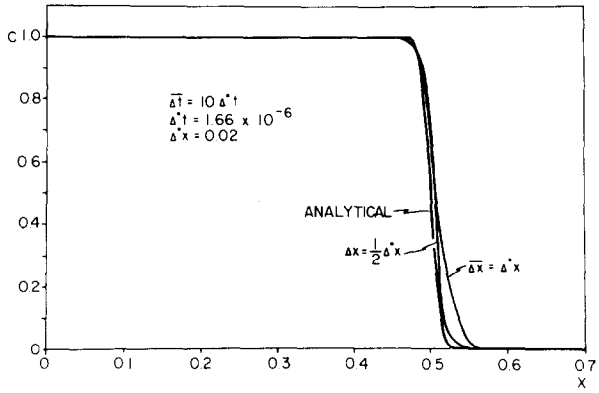

FIG. 6. Results of Example 2 for $t = 5 \times 10^{-5}$ using $\overline{\Delta t} = 1.66\dot{} \times 10^{-5}$ and $\Delta^\circ t = 1.66\dot{} \times 10^{-6}$.

Example 2 is similar to the previous one except that now $D^* = 1.0$, $v = 10^4$, $x_R = 1.0$, and $\Delta^\circ x = 0.02$. The problem is strongly convection-dominated with $Pe = vx_R/D^* = 10^4$. Figure 4 shows that when $\overline{\Delta t} = \Delta^\circ t = 10^{-6}$, the results at $t = 5 \times 10^{-5}$ depend on $\overline{\Delta x}$. When $\overline{\Delta x} = \Delta^\circ x$, there is considerable numerical dispersion. As $\overline{\Delta x}$ decreases, the numerical dispersion diminishes, and when $\overline{\Delta x} = \Delta^\circ x/11$, it almost vanishes. As one may expect, when $\overline{\Delta x} = \Delta^\circ x/2 = v\,\overline{\Delta t}$, the Courant number is 1, and the numerical solution is almost exact (not shown in Fig. 4). The case where the Courant number is equal to 1 is of limited practical interest and will not be considered further in the examples that follow.

If the time steps are made larger so that $\overline{\Delta t} = \Delta^\circ t = 4.54\dot{} \times 10^{-6}$, numerical dispersion is drastically reduced. This is illustrated in Fig. 5, which shows that acceptable results can now be obtained with a coarser convection grid having $\overline{\Delta x} = \Delta^\circ x/3$. The above value of $\overline{\Delta t}$ corresponds to a Courant number of $2.27\dot{}$.

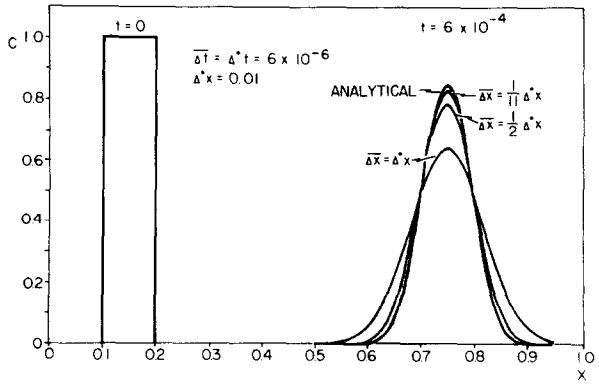

FIG. 7. Results of Example 3 for $t = 6 \times 10^{-4}$ using $\overline{\Delta t} = \Delta^\circ t = 6 \times 10^{-6}$.

According to Fig. 6, a further reduction in numerical dispersion can be achieved by increasing Δt to $1.66' \times 10^{-5}$, while keeping $\Delta^\circ t$ smaller by a factor of 10. This value of Δt corresponds to a Courant number of 8.33'. The results of Example 2 clearly indicate that numerical dispersion can be controlled by refining the convention grid in space, or coarsening it in time, without regard to the Courant–Friedrichs–Lewy condition. Readers interested in comparing our results with those of other methods are referred to Lam [20] and Varoğlu and Finn [47].

Example 3 concerns the convection and dispersion of a rectangular wave. The problem is defined by Eq. (46) subject to

$$\begin{aligned} c(x,0) &= 1 \qquad \text{when} \quad 0.1 \leqslant x \leqslant 0.2 \\ &= 0 \qquad \text{when} \quad 0 < x < 0.1;\ 0.2 < x < 1.0; \\ c(0,t) &= c(1,t) = 0 \end{aligned} \tag{50}$$

and its analytical solution is

$$c(x,t) = \frac{1}{2}\operatorname{erf}\left(\frac{b - x + vt}{2\sqrt{D^* t}}\right) + \frac{1}{2}\operatorname{erf}\left(\frac{b + x - vt}{2\sqrt{D^* t}}\right), \tag{52}$$

where $2b = 0.1$ is the width of the rectangle. The results at $t = 6 \times 10^{-4}$ for $D^* = 1.0$, $v = 10^3$, $\Delta^\circ x = 0.01$, and $\Delta t = \Delta^\circ t = 6 \times 10^{-6}$ are shown in Fig. 7. Large numerical dispersion is obtained when $\Delta x = \Delta^\circ x$, but it reduces rapidly as Δx becomes smaller. However, the tip of the peak remains clipped off even when $\Delta x = \Delta^\circ x/11$. The situation is drastically improved when the time steps are increased by an order of magnitude to $\Delta t = \Delta^\circ t = 5.45' \times 10^{-5}$ (Courant number of 5.45') as shown in Fig. 8. When $\Delta x = \Delta^\circ x/2$, the results are virtually perfect. Results obtained by other methods can be found in Lam [20] and Varoğlu and Finn [47].

Example 4 deals with the pure convection of a rectangular wave identical to that described in Example 3. Here $D^* = 0$, $v = 1$, and even though the dispersion grid is not used, the value of $\Delta^\circ x = 0.01$ is given as a reference. The results for $t = 0.6$ using $\Delta t = 6 \times 10^{-3}$ are shown in Fig. 9. Again, large numerical dispersion is obtained when $\Delta x = \Delta^\circ x$, which diminishes rapidly as Δx becomes smaller. A drastic reduction in numerical dispersion is obtained when Δt is increased by an order of magnitude to $5.45' \times 10^{-2}$ as demonstrated by Fig. 10. The reader may do well to compare our results with those of Lam [20] and Varoğlu and Finn [47, 48].

All the results shown in Figs. 3–10 were obtained by first translating the concentration profile, and then allowing it to disperse, during each Δt. When this sequence was reversed, the results corresponding to the concentration pulses in Figs. 7–10 remained essentially unchanged. However, the concentration fronts corresponding to Figs. 3–6 were now shifted slightly to the right. This shift occurred during the first time step, Δt, and remained essentially unchanged during all later time steps. It appears to have been caused by the left boundary, which prevented the front from dispersing in both directions, to the right *and* to the left, as long as its location coin-

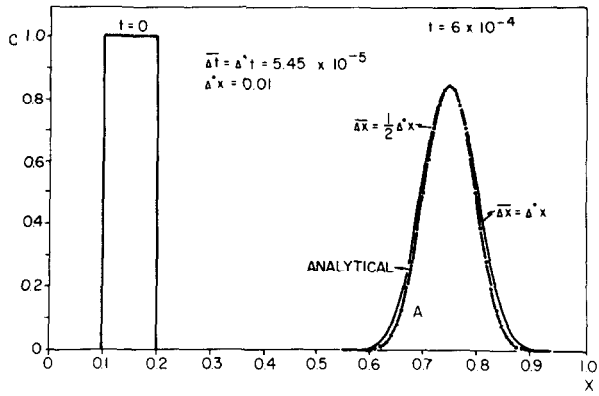

FIG. 8. Results of Example 3 for $t = 6 \times 10^{-4}$ using $\overline{\Delta t} = \Delta^{\circ} t = 5.45^{\cdot} \times 10^{-5}$.

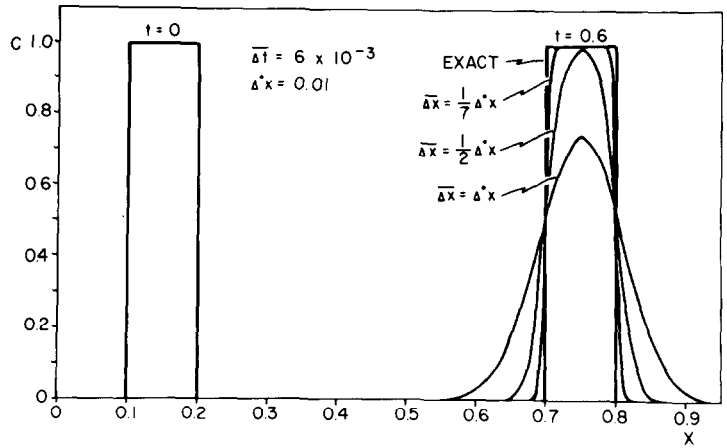

FIG. 9. Results of Example 4 for $t = 0.6$ using $\overline{\Delta t} = 6 \times 10^{-3}$.

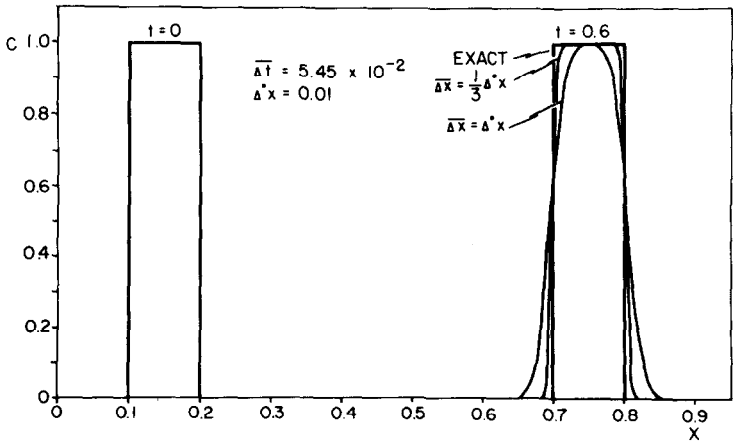

FIG. 10. Results of Example 4 for $t = 0.6$ using $\overline{\Delta t} = 5.45^{\cdot} \times 10^{-2}$.

cided with that of the boundary itself (i.e., during the first $\overline{\Delta t}$). One may conclude from this that when a concentration front is close to an inflow boundary, it is better to translate it before the profile is allowed to disperse.

Example 5 is included to demonstrate the ability of the conjugate grid method to handle problems with variable coefficients. The governing equation is

$$D^* \frac{\partial^2 c}{\partial x^2} - \frac{\partial}{\partial x}[v(x)c] - q(x)c = \frac{\partial c}{\partial t} \qquad \text{on} \quad (x_L, x_R) \times (0, \tau], \tag{53}$$

where $v(x) = -1/x$ and $q(x) = -1/x^2$. When solved subject to the initial and boundary conditions

$$c(x, 0) = 0, \qquad \text{on} \quad (x_L, x_R), \tag{54}$$

$$\frac{\partial c}{\partial x}(x_L, t) = -\frac{2}{x_L} \exp\left(-\frac{x_L^2}{4t}\right), \qquad x_L > 0, \tag{55}$$

$$c(x_R, t) = -Ei\left(-\frac{x_R^2}{4t}\right), \tag{56}$$

the result is

$$c(x, t) = -Ei\left(-\frac{x^2}{4t}\right), \tag{57}$$

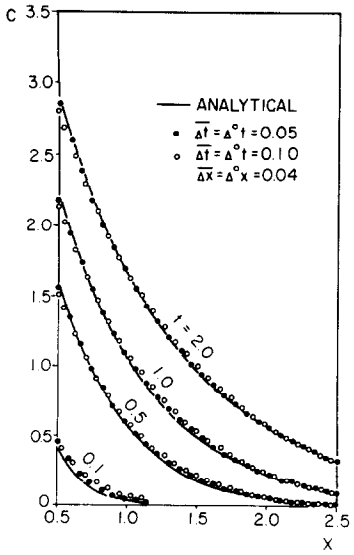

FIG. 11. Results of Example 5.

where Ei is exponential integral. Figure 11 compares the latter with numerical results obtained by the method of dispersion before translation with $D^* = 1$, $x_L = 0.5$, $x_R = 2.5$, $\Delta x = \Delta^\circ x = 0.04$, and $\Delta t = \Delta^\circ t = 0.05$ as well as 0.10 for $t = 0.1$, 0.5, 1.0 and 2.0. Similar results were reported by Varoğlu and Finn [48].

5. Conclusions

The following major conclusions can be drawn from this paper:

1. Lagrangian methods which solve the dispersion–convection equation either on a deforming grid, or on a fixed grid in deforming coordinates, are generally better suited for convection-dominated problems than Eulerian methods based on a fixed grid. On the other hand, the use of a fixed grid in Eulerian coordinates is advantageous when dealing with complex problems involving spatially varying parameters and multiple sources. In addition, a fixed grid can be made compatible with other grids such as those used for computing the velocity field, does not require more than a single evaluation and decomposition of the associated finite difference or finite element matrix in linear problems, and is better suited for the handling of nonlinearities. The purpose of Eulerian–Lagrangian methods is to combine the simplicity of the fixed Eulerian grid with the computational power of the Lagrangian approach.

2. The dispersion–convection equation together with the associated initial and boundary conditions can be formally decomposed into two problems, one involving pure convection, the other being free of convective terms. The "convection problem" can be solved independently at each time step by the method of characteristics applied to a grid fixed in space. The remaining "dispersion problem" can be solved by finite elements on a separate grid which may, but need not, coincide with the former at selected points in space-time. Due to the absence of convective terms, the finite element equations include only symmetric and diagonal matrices. In particular, the matrix coefficient in front of the time derivatives is diagonal and, therefore, the method is amenable to solution by an adaptive mixed explicit–implicit scheme [25–27]. Since the solution of the dispersion problem will often vary in space much more slowly than the actual concentration profile, it can be approximated by means of low-order basis functions defined on a relatively coarse finite element grid. On the

local interpolation.

3. When the conjugate grid method is implemented by linear finite elements and piecewise linear interpolation functions, the results are entirely free of oscillations. This means that there is no overshoot and/or undershoot, so that positive concentration profiles remain positive without suffering from negative "wiggles." This is very important for nonlinear problems such as those arising in some chemically

reacting flows where the loss of positivity may lead to unstable results. The method is also free of phase errors as long as one does not allow sharp fronts to disperse while they coincide with inflow boundaries. While numerical dispersion exists, it can be controlled by reducing the spatial increment or increasing the time step size of the grid associated with the convection problem, the latter measure being the most effective. In contrast to many other methods, best results are often obtained when the time interval exceeds the upper limit allowed by the Courant–Friedrichs–Lewy condition. This is explained by the fact that in the proposed method, numerical dispersion is caused primarily by interpolation between nodes of the convection grid. The larger the time step size, the slower the accumulation of numerical dispersion errors due to such interpolation.

4. Possible improvements worth investigating in the future include the use of higher-order finite elements, higher-order interpolation formulae such as cubic splines for transferring data from one grid to another, and variable interpolation of the kind recommended by Price *et al.* [32]. Another possibility is to allow the convection grid to deform continually while keeping the dispersion grid fixed. Extension of the methodology to two and three spatial dimensions requires further investigation.

ACKNOWLEDGMENTS

The work upon which this paper is based was supported in part by funds provided by the U. S. Department of the Interior, Office of Water Research and Technology, as authorized under the Water Resources Research Act of 1964. Additional support was granted by the U. S. Nuclear Regulatory Commission.

REFERENCES

1. S. W. AHLSTROM, H. P. FOOTE, R. C. ARNETT, C. R. COLE, AND R. J. SERNE, "Multicomponent Mass Transport Model: Theory and Numerical Implementation," Battelle Pacific Northwest Lab. Rept. BNWL-2127, 1977.
2. R. BONNEROT AND P. JAMET, *Internat. J. Numer. Meth. Engrg.* **8** (1974), 811–820.
3. R. BONNEROT AND P. JAMET, *J. Comput. Phys.* **25** (1977), 163–181.
4. D. L. BOOK, J. P. BORIS, AND K. HAIN, *J. Comput. Phys.* **18** (1975), 248–283.
5. J. D. BREDEHOEFT AND G. F. PINDER, *Water Resour. Res.* **9** (1973), 194–210.
6. E. BRESLER, *Water Resour. Res.* **9** (1973), 975–986.
7. N. M. CHAUDHARI, *Soc. Petrol. Engrg. J.* **11** (1971), 277–284.
8. N. M. CHAUDHARI, *Soc. Petrol. Engrg. J.* **13** (1973), 84–92.
9. M. CIMENT, S. H. LEVENTHAL, AND B. C. WEINBERG, *J. Comput. Phys.* **28** (1978), 135–166.
10. A. O. GARDER, D. W. PEACEMAN, AND A. L. POZZI, JR., *Soc. Petrol. Engrg. J.* **4** (1964), 26–36.
11. W. G. GRAY AND G. F. PINDER, *Water Resour. Res.* **12** (1976), 547–555.
12. J. C. HEINRICH, P. S. HUYAKORN, A. R. MITCHELL, AND O. C. ZIENKIEWICZ, *Internat. J. Numer. Meth. Engrg.* **11** (1977), 131–143.
13. P. HINSTRUP, A. KEJ, AND U. KROSZYNSKI, *in* "Proceedings, XVIII Intern. Assoc. Hydraul. Res. Congress, Baden-Baden, Germany, 1977," Vol. 13, pp. 129–137.
14. F. M. HOLLY, JR., AND A. PREISSMANN, *J. Hydraul. Div. ASCE* **103** (1977), 1259–1277.

15. P. S. HUYAKORN, "An Upwind Finite Element Scheme for Improved Solution of the Convection–Diffusion Equation," Rept. 76-WR-2, Water Resources Program, Princeton University, 1976.
16. P. JAMET AND R. BONNEROT, *J. Comput. Phys.* **18** (1975), 21–45.
17. O. K. JENSEN, "Numerical Modelling with a Moving Coordinate System: Application to Flow through Porous Media," Ph. D. dissertation, University of Washington, 1980.
18. O. K. JENSEN AND B. A. FINLAYSON, *Adv. Water Resour.* **3** (1980), 9–18.
19. L. F. KONIKOW AND J. D. BREDEHOEFT, "Computer Model of Two-Dimensional Solute Transport and Dispersion in Ground Water," U. S. Govt. Printing Office, Washington, D. C., 1978.
20. D. C. L. LAM, *in* "Finite Elements in Water Resources" (W. G. Gray, G. F. Pinder, and C. A. Brebbia, Eds.), pp. 1.115–1.129, Pentech, London, 1977.
21. R. B. LANTZ, *Soc. Petrol. Engrg.* **11** (1971), 315–320.
22. D. D. LAUMBACH, *Soc. Petrol. Engrg. J.* **15** (1975), 517–531.
23. S. H. LEVENTHAL, *Soc. Petrol. Engrg. J.* **20** (1980), 120–128.
24. P. MELLI, *in* "Finite Elements in Water Resources" (W. G. Gray, G. F. Pinder, and C. A. Brebbia, Eds.), pp. 1.59–1.69, Pentech, London, 1977.
25. T. N. NARASIMHAN, S. P. NEUMAN, AND A. L. EDWARDS, *Internat J. Numer. Meth. Engrg.* **11** (1977), 325–344.
26. S. P. NEUMAN AND T. N. NARASIMHAN, *Internat. J. Numer. Meth. Engrg.* **11** (1977), 309–323.
27. S. P. NEUMANN, T. N. NARASIMHAN, AND P. A. WITHERSPOON, *in* "Finite Elements in Water Resources" (W. G. Gray, G. F. Pinder, and C. A. Brebbia, Eds.), pp. 1.153–1.186, Pentech, London 1977.
28. K. O'NEILL AND D. R. LYNCH, *in* "Proceedings, 3rd Intern. Conf. on Finite Elements in Water Resources, Univ. of Mississippi, Oxford, 1980," Vol. 1, pp. 3.67–3.76.
29. D. W. PEACEMAN AND H. H. RACHFORD, JR., *Soc. Petrol. Engrg. J.* **2** (1962), 327–339.
30. G. F. PINDER AND H. H. COOPER, JR., *Water Resour. Res.* **6** (1970), 875–882.
31. H. S. PRICE, R. S. VARGA, AND J. R. WARREN, *J. Math. Phys.* **45** (1966), 301–311.
32. H. S. PRICE, J. C. CAVENDISH, AND R. S. VARGA, *Soc. Petrol. Engrg. J.* **8** (1968), 293–300.
33. D. L. REDELL AND D. K. SUNADA, "Numerical Simulation of Dispersion in Groundwater Aquifers," Hydrol. Paper 41, Colorado State University, Ft. Collins, 1970.
34. E. RUNCA AND F. SARDEI, *in* "Atmospheric Environment," Vol. 9, pp. 69–80, Pergamon, Elmsford, N. Y., 1975.
35. A. SETTARI, H. S. PRINCE, AND T. DUPONT, *Soc. Petrol. Engrg. J.* **17** (1977), 228–246.
36. U. SHAMIR AND D. R. F. HARLEMAN, *Water Resour. Res* **3** (1967), 557–581.
37. I. A. SMITH, *in* "Finite Elements in Water Resources" (W. G. Gray, G. F. Pinder, and C. A. Brebbia, Eds.), pp. 1.3–1.20, Pentech, London, 1977.
38. G. D. SMITH, "Numerical Solution of Partial Differential Equations: Finite Difference Methods," 2nd ed., Clarendon, Oxford, 1978.
39. I. M. SMITH, R. V. FARADAY, AND B. A. O'CONNOR, *Water Resour. Res.* **9** (1973), 593–606.
40. H. L. STONE AND P. L. T. BRIAN, *Amer. Inst. Chem. Engrg. J.* **9** (1963), 681–688.
41. M. R. TODD, P. M. O'DELL, AND G. J. HIRASAKI, *Soc. Petrol. Engrg. J.* **12** (1972), 515–530.
42. M. TH. VAN GENUCHTEN, *in* "Finite Elements in Water Resources" (W. G. Gray, G. F. Pinder, and C. A. Brebbia, Eds.), pp. 1.71–1.90, Pentech, London, 1977.
43. M. TH. VAN GENUCHTEN AND P. J. WIERENGA, "Simulation of One-Dimensional Solute Transfer in Porous Media," Agric. Exp. Station Bull. 628, New Mexico State University, Las Cruces, 1974.
44. M. TH. VAN GENUCHTEN, G. F. PINDER, AND E. O. FRIND, *Water Resour. Res.* **13** (1977), 451–458.
45. M. TH. VAN GENUCHTEN AND W. G. GRAY, *Internat. J. Numer. Meth. Engrg.* **12** (1978), 387–404.
46. E. VAROĞLU, *in* "Proceedings, 3rd Intern. Conf. on Finite Elements in Water Resources, Univ. of Mississippi, Oxford, 1980,"Vol. 1, pp. 3.3–3.19.
47. E. VAROĞLU AND W. D. L. FINN, *Adv. Water Resour.* **1** (1978), 337–343.
48. E. VAROĞLU AND W. D. L. FINN, *J. Comput. Phys.* **34** (1980), 371–389.